DFT Insights into the Structural, Mechanical, Electronic and Optical Properties of Novel $InZnCl_3$ and $InCdCl_3$ Chloro-Perovskites

Redi Kristian Pingak[1*], Zakarias Seba Ngara[1], Albert Zicko Johannes[1], Minsyahril Bukit[1], Jehunias Leonidas Tanesib[1], Fidelis Nitti[2], Hery Leo Sianturi[1], and Bartholomeus Pasangka[1]

[1]*Department of Physics, Faculty of Sciences and Engineering, Universitas Nusa Cendana, Jl. Adisucipto Penfui, Kupang 85001, Indonesia*

[2]*Department of Chemistry, Faculty of Sciences and Engineering, Universitas Nusa Cendana, Jl. Adisucipto Penfui, Kupang 85001, Indonesia*

* ***Corresponding author:***

email: rpingak@staf.undana.ac.id

Received: March 15, 2023
Accepted: May 6, 2024

DOI: 10.22146/ijc.94870

Abstract: *The ABX_3 perovskite materials have recently emerged as one of the most promising materials for optoelectronic applications. In the present study, novel perovskites in the form of $InZnCl_3$ and $InCdCl_3$ are computationally investigated to determine their key characteristics, including structural, mechanical, electronic, and optical characteristics. These characteristics were evaluated using the density functional theory (DFT) implemented in the quantum espresso code. The results indicated that both materials exhibit chemical, dynamic, and mechanical stability. Moreover, these perovskites are predicted to be ductile, rendering them suitable for a broad array of optoelectronic applications, including solar cells. The electronic band structure and the density of states of the materials revealed their characteristics as indirect semiconductors with band gap energy values of 0.96 eV for $InZnCl_3$ and 1.83 eV for $InCdCl_3$ perovskites. The optical properties calculations also unveiled that these perovskites possess strong absorption in the visible-ultraviolet spectrum (up to 10^6 cm^{-1}) and low reflectivity. The calculated refractive index and extinction coefficient of the compounds were also predicted in this study. These collective findings strongly suggest the potential applications of these novel materials in optoelectronic devices.*

Keywords: *DFT; Quantum Espresso; perovskite; mechanical property; optoelectronic property*

■ INTRODUCTION

ABX_3 perovskite materials have recently ignited extensive investigation across scientific disciplines as they offer a multitude of advantages compared to conventional semiconductors. Firstly, it is relatively straightforward to tune their electronic and optical properties by A, B, or X ion replacement [1]. This flexibility can lead to a wider or narrower electronic band gap, consequently shifting the absorption energy threshold of the materials to higher or lower photon energy. In addition, these materials offer easy and cost-effective features [2]. Moreover, ABX_3 perovskites also possess unique and remarkable optoelectronic properties [3]. These inherent advantages have established ABX_3 perovskites and their derivatives as highly studied materials for potential applications in a variety of fields including solar cells [4], thermoelectric materials [5], light-emitting diodes [6], scintillation industry [7], lasers [8], photodetectors [9], superconducting applications [10], and gas sensors [11] among others.

Due to their distinctive optoelectronic features, chloro-perovskite materials incorporating chlorine or its combination with other halide anions as the X anion are gaining increasing attention in the materials research community. Numerous experimental investigations have been carried out to comprehensively explore the effects of chlorine on the optoelectronic and photovoltaic performance of perovskites. Chen et al.

[12] discovered that the chlorine incorporation into $CH_3NH_3PbI_3$ perovskite has improved the carrier transport across the hetero-junction interfaces, leading to improved photovoltaic performance of the perovskite. Sun and co-workers [13] further investigated the chemical state of chlorine in perovskites and found a strong correlation between the photovoltaic performance of perovskites and the state of chlorine in the perovskites. The importance of chlorine-based perovskites in optoelectronic field was highlighted in a large number of recent studies including in previous studies [14-16].

In addition to the experimental studies, a large number of computational investigations to find new chloro-perovskites for optoelectronic applications have been conducted in recent years. For instance, Husain and co-workers [17] performed a computational investigation on ternary cubic barium-based chloro-perovskites in the form of $BaMCl_3$ (M = Ag, Cu) and reported that the materials have all the required properties to be applied as absorbers in high frequency applications. Other chloro-perovskites $ABCl_3$ in which A or B are alkaline cations were also intensively studied, including $LiRCl_3$ (R = Be, Mg) [18], $NaXCl_3$ (X = Be, Mg) [19], $XSrCl_3$ (X = Li, Na) [20], $ASiCl_3$ (A = Li, Rb, Cd) [21], $XTiCl_3$ (X = Rb, Cs) [22], $AInCl_3$ (A = K, Rb) [23], $QAgCl_3$ (Q = K, Rb) [24], $RbSrX_3$ (X = Cl, Br) [25], $ACaCl_3$ (A = Cs, Tl) [26], and $CaQCl_3$ (Q = Li, K) [27]. Moreover, recently, computational investigations on other chloro-perovskites in which A and B are other than alkaline cations have been performed. Murshed et al. [28] observed that $TlMgCl_3$ perovskite exhibits exceptional scintillation properties, making it a promising candidate for application in scintillation detectors. Thallium-based chloro-perovskites in the form of $TlMCl_3$ (B = Zn, Cd) [29], $TlSnX_3$ (X = Cl, Br, I) [30], $TlGeCl_xBr_{3-x}$ [31], $TlGeX_3$ (X = Cl, Br, I) [32], and $TlBX_3$ (B = Ge, Sn; X = Cl, Br, I) [33] were also found to possess excellent optoelectronic and thermoelectric applications. These collective studies have highlighted the promising properties of chloro-perovskites for a wide range of applications, strongly emphasizing the significant need for thorough investigation into this class of perovskites.

Indium based chloro-perovskites $InBCl_3$, in particular, have demonstrated considerable potential for optoelectronic and thermoelectric applications. Pingak et al. [34] observed some unique and outstanding optical and thermoelectric features in $InSnCl_3$. Similar findings on $InGeCl_3$ perovskite were also reported in a previous study [35]. Furthermore, other intriguing optoelectronic properties of indium based chloro-perovskites were thoroughly explored in some recent studies including [13,36], unveiling their exciting and long-term prospects.

This study aims to explore some key properties of new indium based chloro-perovskites in the form of $InZnCl_3$ and $InCdCl_3$. These properties include the structural, mechanical, electronic, and optical properties, calculated using the density functional theory (DFT) [37]. The DFT is used in the present article as it has been proven to be highly accurate in predicting the properties of a variety of materials [38-43], especially perovskite materials [44]. As this is the first study conducted on these materials, the obtained results are of significant importance to the fields in which perovskites are applied.

■ EXPERIMENTAL SECTION

The first-principles calculations have been performed using DFT, as implemented in the Quantum Espresso code [45]. The Perdew-Burke-Ernzerhof (PBE) [46] functional was used to parameterize the exchange-correlation while the ultrasoft pseudopotential was used to take into account the electron-nuclei interactions within the constituent atoms of the compounds. The convergence in the total energy of the perovskites was reached when the energy difference between two consecutive self-consistent calculations was less than 10^{-8} Ry. K-points of $6 \times 6 \times 6$ and $12 \times 12 \times 12$ have been adopted for Self-Consistent Field (SCF) and Non-Self-Consistent Field (NSCF) calculations, respectively. The energy cut-off values used for the wave function and the charge density were 60 and 480 Ry, respectively. Moreover, the thermo_pw code, linked with the Quantum Espresso, was used to calculate the optical and elastic properties of the materials.

■ RESULTS AND DISCUSSION

Structure

The cubic $InZnCl_3$ and $InCdCl_3$ crystalize in the space group pm$\bar{3}$m (#221). The unit cell structure of $InCdCl_3$ is visualized in Fig. 1, where In cations occupy the Wyckoff coordinates of (0,0,0) while Cd is located at (0.5,0.5,0.5). The three Cl anions are positioned at (0.5,0,0.5), (0.5,0.5,0), and (0,0.5,0.5). The unit cell structure of $InZnCl_3$ is identical to that of the $InCdCl_3$, with Zn occupying the Cd position.

The Birch-Murnaghan equation of states [47], presented in Eq. (1), was used to optimize the crystal structure of the perovskites. In Eq. (1), V_0 is the optimized volume; a_0 is the optimized lattice parameter, B and B' are the bulk modulus and its pressure derivative, respectively, and E_0 is the total energy. The fitting results of the equation are displayed in Fig. 2 with numerical values listed in Table 1, where the optimized lattice constants are also presented.

$$E(V) = E_0 + \frac{B}{B'(B'-1)}\left[V\left(\frac{V_0}{V}\right)^{B'} - V_0\right] + \frac{B}{B'}(V - V_0) \qquad (1)$$

It can be seen from Fig. 2 that the equilibrium unit cell of the optimized $InCdCl_3$ structure is larger than that of $InZnCl_3$ material, which is expected as the ionic radius of Cd is larger than that of Zn. The optimized lattice constants of $InZnCl_3$ and $InCdCl_3$ are found to be 4.97 and 5.25 Å, respectively. The increase in the lattice constant as Cd replaces Zn was also reported for the isoelectronic compounds in the form of $TlZnCl_3$ (4.98 Å) and $TlCdCl_3$ (5.26 Å) [29]. This trend is also true for various ABX_3 perovskites where A and B cations are substituted with their larger counterparts including $XZnI_3$ [48], $XAlN_3$ [49], $AGeF_3$ [50], $LiXF_3$ [51], $BeXH_3$ [52], $TlBF_3$ [53], $AGeF_3$ [54], $TlXF_3$ [55], and $XMgF_3$ [56]. Similarly, various studies have also predicted a systematic increase in the lattice parameters as X anions were replaced by larger size anions such as $CsGeX_3$ [57], $NaGeX_3$ [58], and $BaLiX_3$ [59]. The predicted equilibrium densities of the two materials reveal that $InCdCl_3$ (3.94 g/cm^3) is denser than $InZnCl_3$ (3.81 g/cm^3).

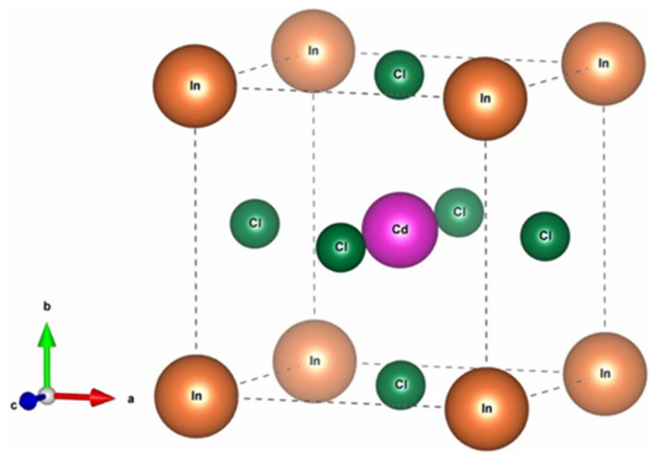

Fig 1. The unit cell structure of cubic $InCdCl_3$ perovskite material

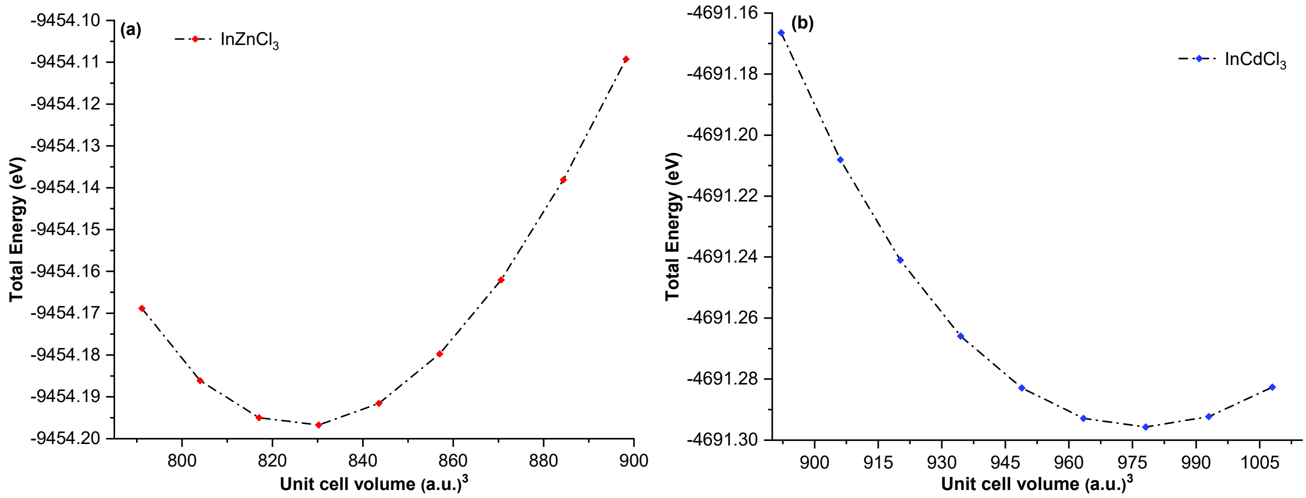

Fig 2. Total energy vs unit cell volume of (a) $InZnCl_3$ and (b) $InCdCl_3$ perovskites

Table 1. The structural parameters of the cubic $InZnCl_3$ and $InCdCl_3$ perovskites

Perovskite	V_0 (a.u.)^3	a_0 (Å)	B (GPa)	B'	E_0 (eV)	ρ_0 (g/cm^3)
$InZnCl_3$	826.74	4.97	36.20	5.10	-9454.20	3.81
$InCdCl_3$	977.45	5.25	31.40	4.72	-4691.25	3.94

Chemical and Dynamic Stability

To investigate the chemical stability of the compounds, their formation energies have been calculated using Eq. (2).

$$\Delta E_f = E_{tot}(\ln BCl_3) - E(\ln) - E(B) - 3E(Cl) \quad (2)$$

Here, E_{tot} ($InBCl_3$) is the total energy of the $InBCl_3$ (B = Zn, Cd) perovskites whereas the energy of individual atoms In, B (Zn, Cd), and Cl is denoted by E(In), E(B), and E(Cl), respectively. It is found that the formation energy values of $InZnCl_3$ and $InCdCl_3$ are −13.20 and −12.79 eV, respectively. The negative formation energy implies that these materials possess chemical stability and can be experimentally synthesized under ambient conditions. It should also be noted that the formation energy as defined in Eq. (2), assumes that the materials are synthesized from their elemental atoms in gas phase, i.e., Cl, Cd or Zn, and In atom. The formation energy of materials can also be calculated using the elemental most stable phase energy or chemical potential, as presented in a previous study [60].

Another important property of these materials is their dynamic stability, which can be evaluated from their phonon dispersion curve (Fig. 3). As there are five atoms in a unit cell of $InBCl_3$ (B =Zn, Cd) perovskites, it is expected that there will be 15 phonon modes in the phonon dispersion. These modes consist of twelve acoustic modes and three optical modes. The three optical modes are clearly seen in the case of $InCdCl_3$ (Fig. 3(b)) as there is an obvious gap between the acoustic and the optical branches. On the other hand, two of the three optical modes in $InZnCl_3$ overlap with the acoustic ones. Similarly, some acoustic modes cannot be seen in particular directions due to the degeneracy of some modes. For instance, only eight acoustic modes are observed in the Γ – X, R – M, and Γ – R directions, meaning that the four other modes are degenerate with some of the eight acoustic modes appearing in Fig. 3. Meanwhile, all twelve modes are seen in X – M, M – Γ, and R – X directions, suggesting the non-degeneracy of the modes.

The absence of negative frequencies in Fig. 3(a) and 3(b) suggests that the two materials are dynamically stable. The dynamic stability of a material is generally indicated by the positive vibrational modes, accompanied by the presence of three vibrational modes at the Γ point symmetry [61]. This is true in the present work, strongly indicating the dynamic stability of the perovskites.

Mechanical Properties

The calculated elastic constants of the studied materials along with other mechanical properties are summarized in Table 2.

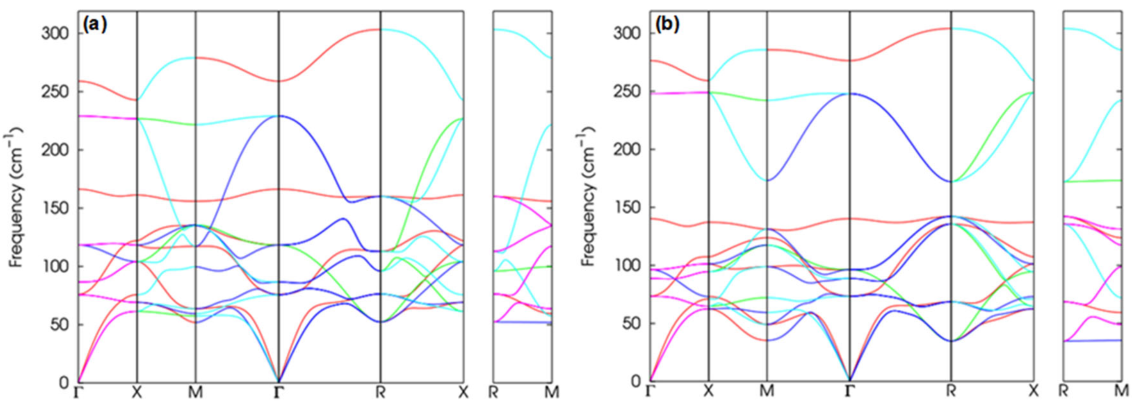

Fig 3. Phonon dispersion curve of (a) $InZnCl_3$ and (b) $InCdCl_3$ perovskites

Table 2. Elastic constants C_{ij} and mechanical properties of cubic $InBCl_3$ (B = Zn, Cd) perovskites

Parameter	$InZnCl_3$	$InCdCl_3$
C_{11} (GPa)	54.18	55.49
C_{12} (GPa)	25.73	19.20
C_{44} (GPa)	19.04	9.17
Cauchy pressure (C_{11}-C_{12})	28.45	36.29
Bulk modulus, B (GPa)	35.21	31.30
Shear modulus, G (GPa)	16.94	12.09
Young modulus, E (GPa)	43.80	32.13
Pugh ratio, B/G	2.08	2.59
Poisson ratio, ϑ	0.29	0.33
Debye temperature, θ_D (K)	238.54	191.39

One of the most important mechanical properties that can be obtained from the calculated elastic properties of the compounds is their mechanical stability. The Born-Huang mechanical stability criteria [62] were adopted in this study to evaluate the mechanical stability of the compounds. Since the elastic constants of both materials satisfy $C_{11} > 0$, $C_{44} > 0$, $(C_{11}-C_{12}) > 0$, $(C_{11} + 2C_{12}) > 0$, and $C_{12} < B < C_{11}$, they are mechanically stable. This is an important finding as in general, there are three main factors affecting the mechanical stability of the perovskites layer in practical applications: the intrinsic characteristics of the perovskite, the effect of the other layers in the devices, and the absence or presence of a protective layer [63]. This means that since $InZnCl_3$ and $InCdCl_3$ are projected to possess intrinsic mechanical stability, their performance in devices can be optimized only by considering the two external factors.

The ductility and brittleness of materials are also important for their practical applications in optoelectronic devices because ductile materials can be easily deposited into thin films [64]. In order to investigate the ductile or brittle behavior of the perovskites under study, their Poisson ratio has been computed and the results are listed in Table 2. The Poisson ratio of $InZnCl_3$ is 0.29 while that of $InCdCl_3$ is 0.33. According to [65], materials with a Poisson ratio larger than 0.26 are considered as ductile. Thus, our results indicate that both $InZnCl_3$ and $InCdCl_3$ are ductile in nature. This can be further confirmed by analyzing their Pugh ratio: ductile materials should have Poisson ratio larger than 1.75 and vice versa [66]. As indicated in Table 2, the calculated Pugh ratio values for $InZnCl_3$ and $InCdCl_3$ are 2.08 and 2.59, confirming their ductile behavior. The Cauchy pressure is another elastic parameter that can also be used to confirm the ductility of the studied perovskites. Materials with ductile nature generally possess positive Cauchy pressure [67]. Table 2 provides clear evidence that both compounds have positive Cauchy pressure. Therefore, it can be confidently inferred that the two materials are ductile, with $InCdCl_3$ predicted to be more ductile than $InZnCl_3$. This ductile behavior makes them promising candidates for applications as thin films in optoelectronic devices.

The calculated mechanical moduli of the perovskites are also presented in Table 2. The first one is the bulk modulus, which measures the resistance of a material to compression. The results showed that $InZnCl_3$ and $InCdCl_3$ have high bulk moduli of 54.18 and 55.49 GPa, respectively. The similarity in the bulk moduli of the two compounds suggests that they will exhibit approximately similar responses to applied compression. The calculated bulk moduli of $InZnCl_3$ and $InCdCl_3$ are significantly larger than those of other chloroperovskites reported in the literature, including $NaBeCl_3$ (20.56 GPa) and $NaMgCl_3$ (20.59 GPa) [19] as well as $LiBeCl_3$ (45.15 GPa) and $LiMgCl_3$ (33.36 GPa) [18]. As seen from Table 2, the shear modulus of the $InZnCl_3$ is 16.94 GPa, considerably larger than that of $InCdCl_3$ (12.09 GPa). This indicates that $InZnCl_3$ is projected to be more resistant to shear deformation compared to $InCdCl_3$. This is also true for their isoelectronic compounds namely $TlZnCl_3$ and $TlCdCl_3$ [29], with shear moduli of 17.47 and 12.33 Gpa, respectively. Similarly, the calculated Young modulus of $InZnCl_3$ (43.80 GPa) is significantly larger than that of $InCdCl_3$ (32.13 GPa). The large difference in the Young modulus was also predicted for $TlZnCl_3$ (44.91 GPa) and $TlCdCl_3$ (32.33 GPa) [29].

Electronic Features

The calculated electronic band structure and the total density of states (TDOS) of $InZnCl_3$ and $InCdCl_3$ are displayed in Fig. 4. The general features of the band

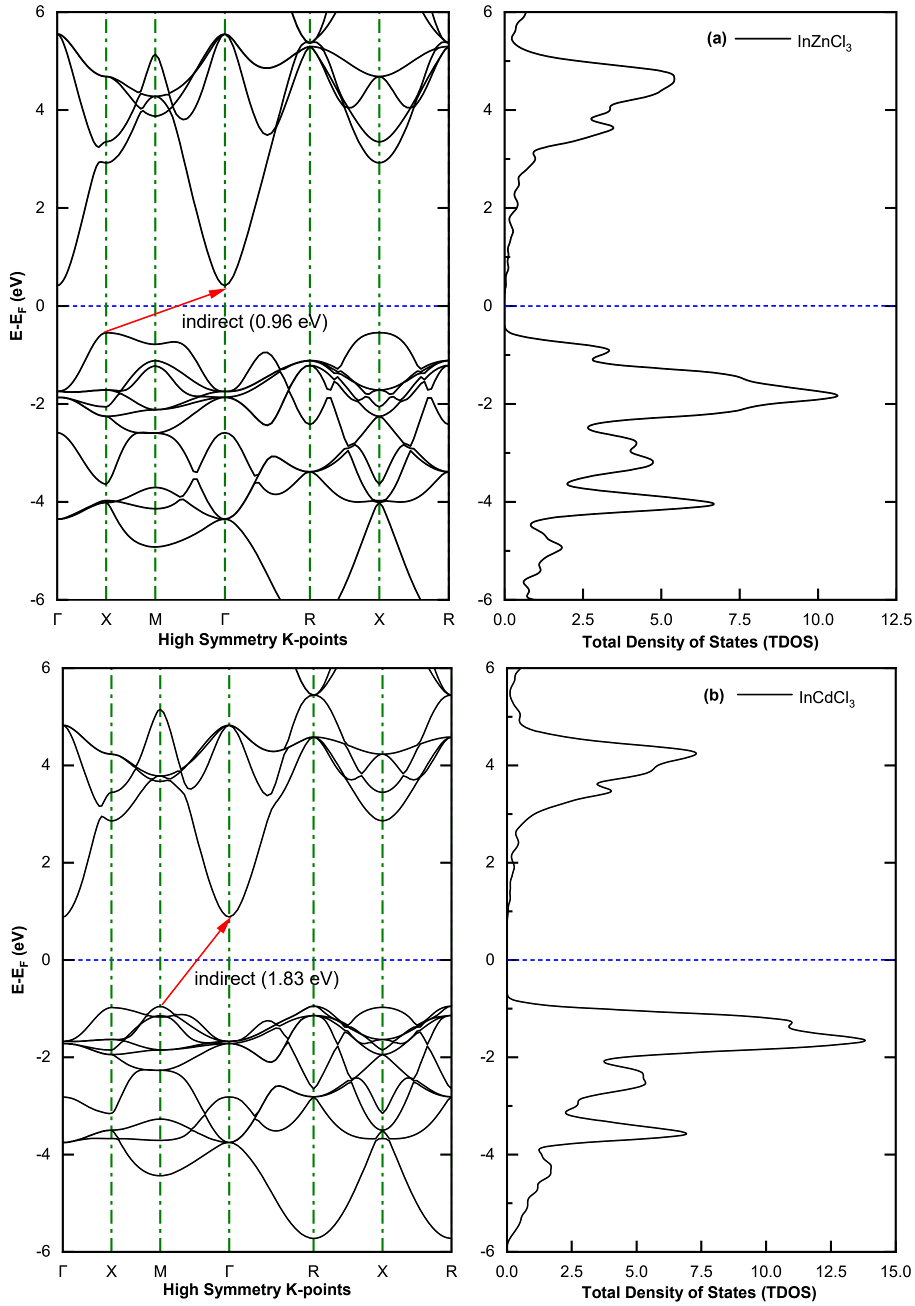

Fig 4. Electronic band structure and TDOS of cubic (a) $InZnCl_3$ and (b) $InCdCl_3$ perovskites

structure and the TDOS of the two compounds are very similar, as expected. A notable difference observed is a shift of states in both the valence and conduction bands, moving away from the Fermi energy as Cd replaces Zn. This leads to a wider forbidden gap of 1.83 eV (M→Γ) for $InCdCl_3$, almost twice that of $InZnCl_3$ with band gap of 0.96 eV (X→Γ). Nevertheless, the two materials are categorized as semiconductors. It is true that the use of hybrid functionals and Coulomb energy correction (U) can improve the accuracy of the energy gap values generated from the PBE functional, as presented in previous studies [68]. However, the PBE functional was also proven to have approximately the same level of accuracy as more computationally expensive functionals in predicting the lattice constants of some materials [69]. Indeed, PBE could produce more reliable lattice constants compared to those predicted by other functionals [69].

The widening of the band gap of ABX_3 compounds as larger A or B cations replace the position of the smaller ones was observed for a variety of perovskites including A_2NaIO_6 [70], $A_2ScCuCl_6$ [71], Sr_3MN [72], Ba_2MWO_6 [73], and Cs_2BBr_6 [74]. Similarly, the observation is also true when X anions are substituted by other isoelectronic counterparts with larger ionic radii such as Rb_2AuBiX_6 [75], $CsInSbAgX_6$ [76], $CsRbPtX_6$ [77], Rb_2PtX_6 [78], K_2CuBiX_6 [79], and Cs_2RbSbX_6 [80]. The band gap modulation can also be obtained by applying hydrostatic or uniaxial pressure, as reported in a previous study [81]. The above-mentioned studies clearly indicate that perovskites are highly tunable enabling facile adjustment of their optoelectronic properties to obtain desired characteristics for specific applications across a broad spectrum of devices. The band gap values of the perovskites should be experimentally verified before they are used in practical applications. The Tauc plot method is one of the most commonly used methods for the experimental calculation of the band gap of materials [82].

It is interesting to note that the widening of the band gap of the materials as Cd replaces Zn is not followed by an increase in the bulk moduli of the compounds. This is in contrast to the results reported by Reddy et al. [83], who observed a systematic relationship between the bulk modulus and the band gap energy for some materials. They reported that the band gap energy is linearly proportional to the bulk moduli of the materials. Therefore, the inverse relationship of the two materials obtained in this study is interesting and could provide some interesting physical phenomena. Similar trend was also reported in a study [84], which stated that there is a large variation in band gap of alloys owing to chemical and size effects. As a result, the bulk moduli of alloys are not always linearly proportional to their band gap energy [84].

The contribution of the valence electrons' states of all constituent atoms in the valence and conduction bands of $InZnCl_3$ and $InCdCl_3$ are explored through the partial density of states (PDOS) diagram, depicted in Fig. 5(a) and 5(b) for the respective perovskites. Overall, no significant change was observed in the shape of the orbitals except for the widening of the forbidden energy range between the valence and conduction band, confirming the band structure and TDOS diagrams (Fig. 4). It is obvious that closest to the Fermi level, Cl-3p makes the most significant contribution in the valence bands of both compounds, followed by the In-5s orbital. The next contribution in this energy region comes from the Zn-3d orbital (for $InZnCl_3$) and Cd-4d orbital (for $InCdCl_3$), with a much lower proportion. On the other hand, Zn-4s and Cd-5s are the most dominant states in the conduction band region closest to the Fermi level. These are the states that are expected to take part in any electronic transition from the valence band to the conduction band of the materials. These findings are also

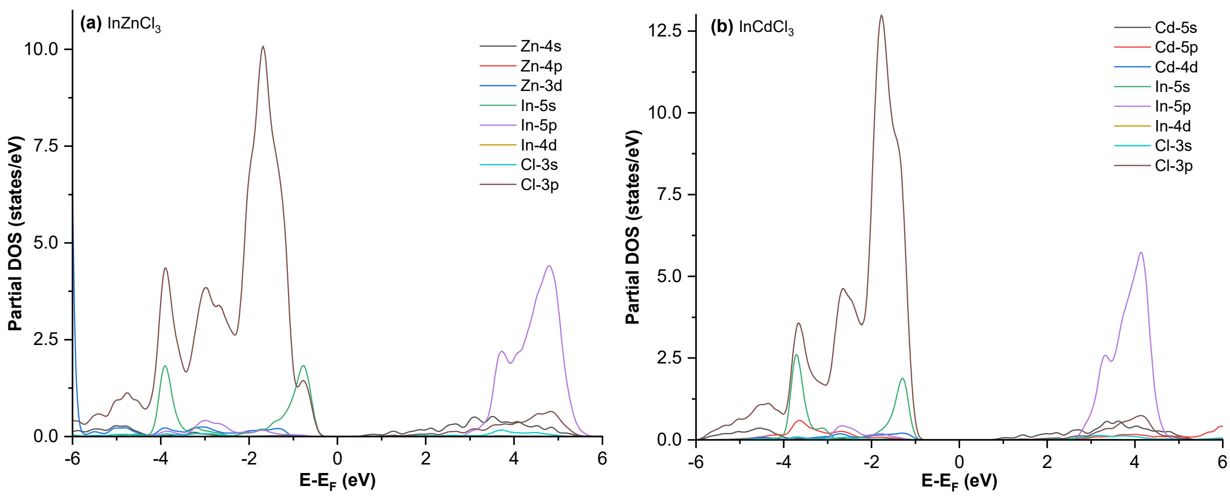

Fig 5. PDOS of cubic (a) $InZnCl_3$ and (b) $InCdCl_3$ perovskites

consistent with those reported in a study [29] for isoelectronic perovskites $TlZnCl_3$ and $TlZnCd_3$.

The (110) electronic density map of the perovskites under study is shown in Fig. 6. The electron distribution around Cl and In atoms is nearly spherical, indicating that In–Cl bond is nearly ionic in nature. On the other hand, the electronic density is distorted between Cl and Zn (or Cd) atoms, implying a more covalent nature of Cl–Zn and Cl–Cd bond. The Cl–Cd covalent bond is projected to be stronger than the Cl–Zn bond, as seen from the denser electron distribution between Cl and Cd compared to the region between Cl and Zn. This has been anticipated as Zn and Cd possess different ionic sizes, with Cd being the largest cation. This means that the electrical polarization experienced by Cd in the presence of the Cl ion is of greater magnitude compared to the polarization experienced by Zn. As a result, more electrons are localized in the regions between the Cd and Cl compared to those between Zn and Cl. The electronic distribution of isoelectronic compounds $TlBCl_3$ (B = Zn, Cd) was not reported in a previous study [29]. Therefore, a direct comparison cannot be presented in this work.

Optical Properties

The optical properties of the studied perovskites for photon energy between 0 and 20 eV have been calculated in this study. Equations used to calculate these properties can be found elsewhere [59]. In order to calculate all optical properties of the materials, their dielectric functions consisting of the real part $\varepsilon_1(\omega)$ and the imaginary part $\varepsilon_2(\omega)$ were first calculated, with the results visualized in Fig. 7. A comparison of the dielectric function of the two compounds shows an apparent similarity across the entire photon energy range. A close similarity is also true when comparing it with the dielectric functions of $TlZnCl_3$ and $TlCdCl_3$ [29],

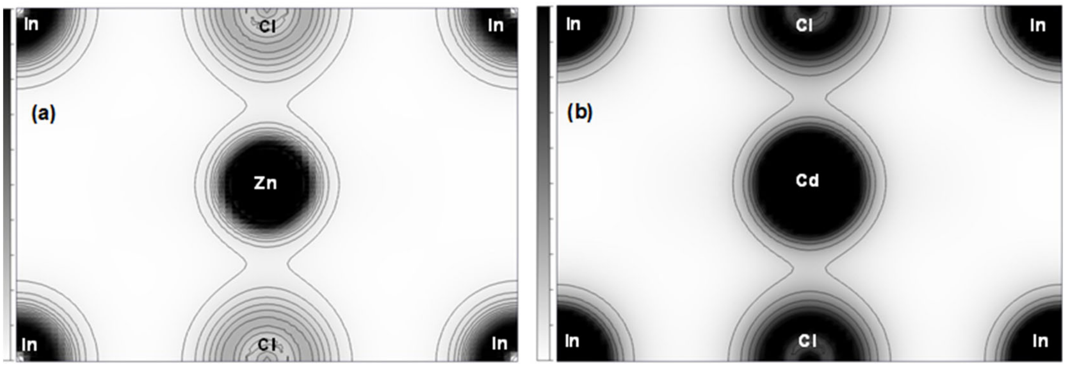

Fig 6. (110) Electronic density cubic (a) $InZnCl_3$ and (b) $InCdCl_3$ perovskites

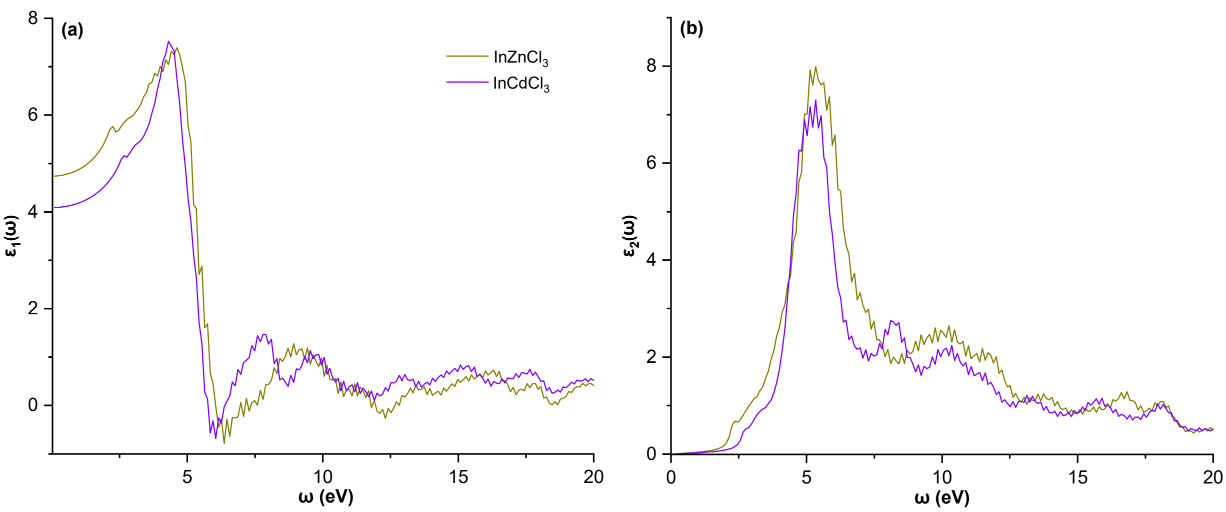

Fig 7. (a) $\varepsilon_1(\omega)$ and (b) $\varepsilon_2(\omega)$ of cubic $InZnCl_3$ and $InCdCl_3$ perovskites

indicating that these materials exhibit similar responses to incident light. However, two of the most important aspects which should be noted are $\varepsilon_1(0)$ and the energy at which $\varepsilon_2(\omega)$ starts rising.

The $\varepsilon_1(0)$ value, which is the static dielectric function, can be used to predict the performance of a material for application in optoelectronic devices. Materials with larger $\varepsilon_1(0)$ values generally exhibit better performance in optoelectronic applications [85]. It is found that $InZnCl_3$ has a larger $\varepsilon_1(0)$ value of 4.74, compared to $InCdCl_3$ whose $\varepsilon_1(0)$ value is predicted to be 4.09 (Fig. 7a). These findings are also consistent with Penn's model [86], stating that electronic band gap of materials is inversely proportional to their static dielectric function. This agreement is, therefore, a validation of our results. Furthermore, the highest peaks of $\varepsilon_1(\omega)$, the two compounds appear at nearly the same energy and exhibit similar magnitudes. The highest figure for $InZnCl_3$ is 7.39 at 4.62 eV and that for $InCdCl_3$ is 7.32 at 4.31 eV.

The imaginary part of the dielectric function ($\varepsilon_2(\omega)$) is a measure of the absorption behavior of a material. Therefore, it can be used to predict the energy at which a material initiates absorbing incident light, which should closely correlate with the magnitude of electronic forbidden gap. Materials with a lower electronic band gap are expected to absorb light at lower photon energy. This is true in the present work, where it is found that $InZnCl_3$ (band gap of 0.96 eV) has lower energy threshold energy for $\varepsilon_2(\omega)$ than that of the $InCdCl_3$ (band gap of 1.83 eV). From this threshold energy, $\varepsilon_2(\omega)$ experiences considerable increase, reaching a maximum value of 7.99 at 5.33 eV for $InZnCl_3$ and 7.30 also at 5.33 eV for $InCdCl_3$. Subsequently, the function declines for higher energy values.

The calculated dielectric function of the compounds was then used to determine other optical attributes including the reflectivity $R(\omega)$, the refractive index $n(\omega)$, the absorption coefficient $\alpha(\omega)$, and the extinction coefficient $k(\omega)$. The results are displayed in Fig. 8(a), 8(b), 8(c), and 8(d), respectively.

As depicted in Fig. 8(a), very low reflectivity values are predicted for the materials, especially around the optical threshold energy. Within [0,2.5] eV, the reflectivity ranges from 13.73% to 17.21% for InZnCl3 and 11.43% to 14.94% for $InCdCl_3$. This implies a minimal energy loss due to the reflection of light from the surface of the two materials, which is favorable for optoelectronic devices requiring minimal reflectivity. It is predicted that $InZnCl_3$ will exhibit a maximum reflectivity of 35.29% at 5.85 eV, similar to $InCdCl_3$, which also shows the highest reflexivity of 33.78% at 5.85 eV. Subsequently, the reflectivity of the two materials reduces with some fluctuations for higher photon energy, reaching the minimum values of 5.10% and 2.98% for $InZnCl_3$ and $InCdCl_3$ perovskites, respectively.

Fig. 8(b) shows the refractive index of $InBCl_3$ (B = Zn, Cd) as a function of the photon energy $\eta(\omega)$. A considerable similarity between $\eta(\omega)$ and $\varepsilon_1(\omega)$ (Fig. 7(a)) can be readily observed, which is expected. Lamichhane and Ravindra [87] developed an empirical model to relate various perovskite materials' refractive index and energy gap. The authors found that the energy gap values of materials are generally smaller for materials with larger refractive index. The authors observed that their model is in excellent agreement with some well-established models in the literature. The model demonstrates good performance in the current study, where it is found that $InZnCl_3$ (E_g = 0.96 eV) has a larger static refractive index of 2.18, compared to 2.02 of $InCdCl_3$ (E_g = 1.83 eV). It can also be observed from Fig. 8(b) that the refractive index of the studied perovskites increases, reaching a maximum value of 2.86 at 4.92 eV ($InZnCl_3$) and 2.84 at 4.51 eV ($InCdCl_3$). Subsequently, the refractive index decreases for higher values of the photon energy.

Fig. 8(c) displays the absorption coefficient $\alpha(\omega)$ of the perovskites as a function of the photon energy. It indicates that the materials possess really strong absorption, reaching 10^6 cm^{-1}. This observation has been anticipated as the materials possess low reflectivity as shown in Fig. 8(a). Strong absorption is one of the most essential requirements for materials to be applied as absorbers in optoelectronic devices. The energy threshold for the absorption is consistent with the electronic band gap, where $InZnCl_3$ is predicted to start

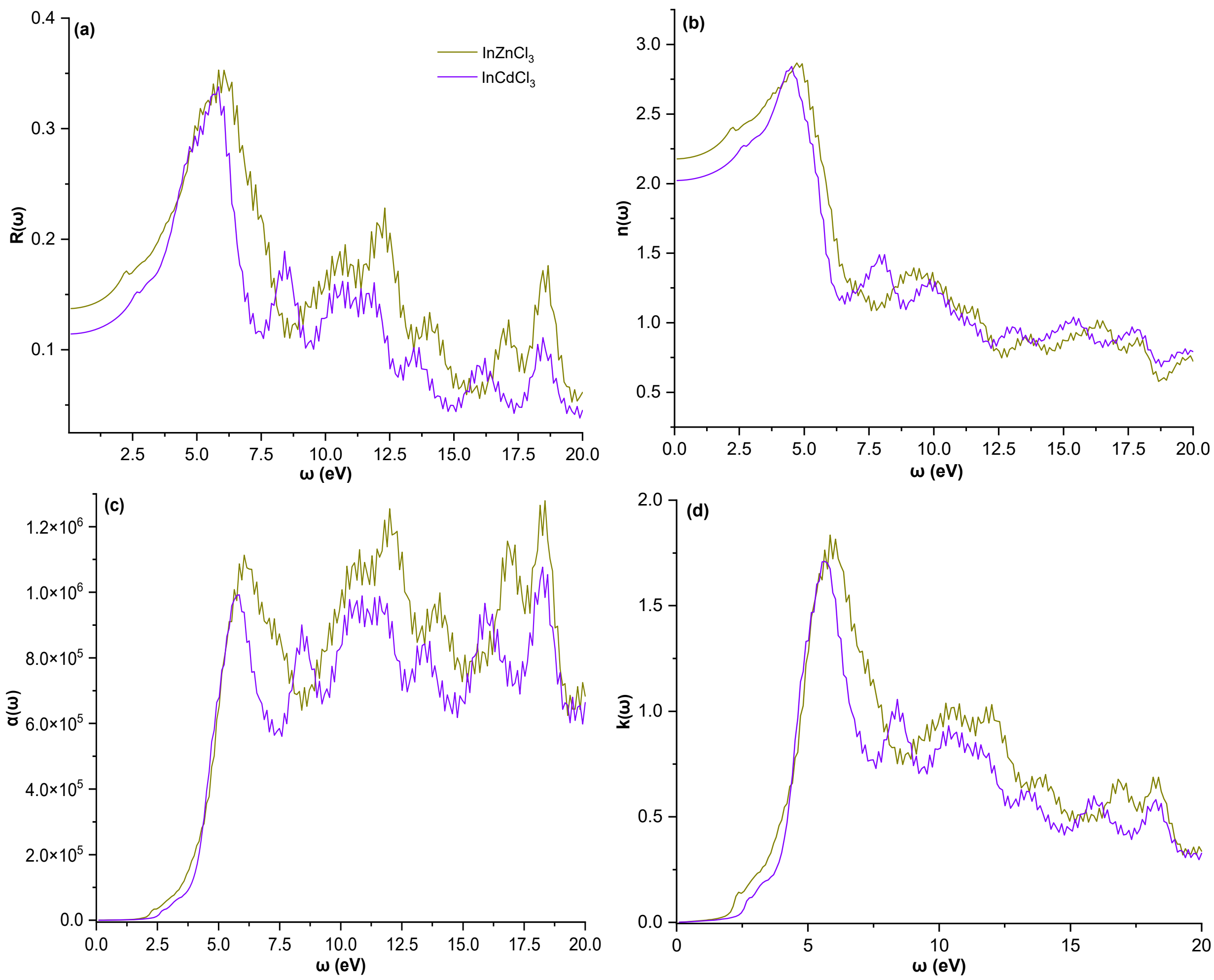

Fig 8. (a) R(ω), (b) n(ω), (c) α(ω), and (d) k(ω) of cubic $InZnCl_3$ and $InCdCl_3$ perovskites

absorbing light at lower energy than $InCdCl_3$. This trend has also been reported for $TlZnCl_3$ and $TlCdCl_3$ [29]. This exceptional absorption behavior has also been predicted for a large number of perovskites including $Ba_3CaNb_2O_9$ [88], $LiCaF_3$ [89], $RbGeBr_3$ [90], and $RbSrX_3$ [91].

Closely related to the absorption coefficient α(ω) and $\varepsilon_2(\omega)$ is the extinction coefficient k(ω), presented in Fig. 8(d). A comparison of Fig. 7(b), Fig. 8(c), and Fig. 8(d) reveals a remarkable similarity among the three parameters in the energy interval of [0,2.5] eV. This confirms that $InZnCl_3$ is more favorable than $InCdCl_3$ for optoelectronic applications in lower photon energy ranges such as solar cells. The highest peak of the extinction coefficient of $InZnCl_3$ appears at 5.85 eV (with maximum value of 1.83) while that of $InCdCl_3$ is observed at 5.74 eV (with a maximum value of 1.71). Further work will include the synthesis of the materials to verify their properties before they are employed in optoelectronic devices. It should be noted that although the materials are predicted to possess excellent optoelectronic properties, achieving their best performance for practical optoelectronic applications is challenging. A number of factors might affect the materials' performance in devices such as intrinsic point defects [92], hydrogen-induced nonradiative recombination [93], oxygen ingression [94], and H_i^+ ion diffusion [95]. These factors must be considered when real applications of the materials are made.

■ CONCLUSION

The present study successfully implemented the DFT to explore the structural, mechanical, electronic, and optical properties of new materials $InZnCl_3$ and $InCdCl_3$. The results revealed that the proposed materials are chemically and thermodynamically stable in the cubic structure with optimized lattice constants of 4.97 and 5.25 Å for the respective compounds. The evaluation of their elastic constants further demonstrated that the materials exhibit mechanical stability and possess ductile behavior in nature. From the electronic band structure and the density of states, it was found that both $InZnCl_3$ and $InCdCl_3$ are indirect semiconductors with band gap values of 0.96 and 1.83 eV, respectively. The results also indicated that the materials exhibit excellent optical behaviors including highly strong absorption in the visible and ultraviolet electromagnetic spectrum and low reflectivity. Given their promising potential for optoelectronic applications, it is recommended that experimental studies be conducted to validate these predicted properties prior to their applications in various devices.

■ ACKNOWLEDGMENTS

The authors thank the Faculty of Science and Engineering, University of Nusa Cendana, for providing full funding for this research through *Penelitian Dasar Unggulan Perguruan Tinggi* (PDUPT) scheme in 2024 (Contract Number: 6/UN15.18.PPK/SPP/FST/IV/2024).

■ CONFLICT OF INTEREST

The authors do not have a conflict of interest.

■ AUTHOR CONTRIBUTIONS

Redi Kristian Pingak wrote the original draft of the manuscript and conducted the DFT calculation. Redi Kristian Pingak, Zakarias Seba Ngara, Albert Zicko Johannes, Minsyahril Bukit, and Jehunias Leonidas Tanesib analyzed and interpreted the results. Fidelis Nitti analyzed the results and revised the manuscript. Hery Leo Sianturi and Bartholomeus Pasangka revised the manuscript. All authors agreed to the final version of this manuscript.

■ REFERENCES

[1] Anaya, M., Lozano, G., Calvo, M.E., and Míguez, H., 2017, ABX_3 Perovskites for tandem solar cells, *Joule*, 1 (4), 769–793.

[2] Zhang, L., Mei, L., Wang, K., Lv, Y., Zhang, S., Lian, Y., Liu, X., Ma, Z., Xiao, G., Liu, Q., Zhai, S., Zhang, Shengli, Liu, G., Yuan, L., Guo, B., Chen, Z., Wei, K., Liu, A., Yue, S., Niu, G., Pan, X., Sun, J., Hua, Y., Wu, W.Q., Di, D., Zhao, B., Tian, J., Wang, Z., Yang, Y., Chu, L., Yuan, M., Zeng, H., Yip, H.L., Yan, K., Xu, W., Zhu, L., Zhang, W., Xing, G., Gao, F., and Ding, L., 2023, Advances in the application of perovskite materials, *Nano-Micro Lett.*, 15 (1), 177.

[3] Zhou, Y., Wang, J., Luo, D., Hu, D., Min, Y., and Xue, Q., 2022, Recent progress of halide perovskites for thermoelectric application, *Nano Energy*, 94, 106949.

[4] Green, M.A., Ho-Baillie, A., and Snaith, H.J., 2014, The emergence of perovskite solar cells, *Nat. Photonics*, 8 (7), 506–514.

[5] Haque, M.A., Kee, S., Villalva, D.R., Ong, W.L., and Baran, D., 2020, Halide perovskites: Thermal transport and prospects for thermoelectricity, *Adv. Sci.*, 7 (10), 1903389.

[6] Kim, J.S., Heo, J.M., Park, G.S., Woo, S.J., Cho, C., Yun, H.J., Kim, D.H., Park, J., Lee, S.C., Park, S.H., Yoon, E., Greenham, N.C., and Lee, T.W., 2022, Ultra-bright, efficient and stable perovskite light-emitting diodes, *Nature*, 611 (7937), 688–694.

[7] Wibowo, A., Sheikh, M.A.K., Diguna, L.J., Ananda, M.B., Marsudi, M.A., Arramel, A., Zeng, S., Wong, L.J., and Birowosuto, M.D., 2023, Development and challenges in perovskite scintillators for high-resolution imaging and timing applications, *Commun. Mater.*, 4 (1), 21.

[8] Qin, C., Sandanayaka, A.S.D., Zhao, C., Matsushima, T., Zhang, D., Fujihara, T., and Adachi, C., 2020, Stable room-temperature continuous-wave lasing in quasi-2D perovskite films, *Nature*, 585 (7823), 53–57.

[9] Zhan, X., Zhang, X., Liu, Z., Chen, C., Kong, L., Jiang, S., Xi, S., Liao, G., and Liu, X., 2021, Boosting the performance of self-powered $CsPbCl_3$-based UV photodetectors by a sequential vapor-deposition strategy and heterojunction engineering, *ACS Appl. Mater. Interfaces*, 13 (38), 45744–45757.

[10] Shahzad, M.K., Hussain, S., Farooq, M.U., Abdullah, A., Ashraf, G.A., Riaz, M., and Ali, S.M., 2024, First principle investigation of tungsten based cubic oxide perovskite materials for superconducting applications: A DFT study, *J. Phys. Chem. Solids*, 186, 111813.

[11] Zhang, H., Zhang, L., Zhao, Z., Xin, W., Niu, J., He, J., and Jiao, W., 2024, A sensitive $CsBr/Cs_3Bi_2Br_3I_6$ heterostructure perovskite gas sensor for H_2S detection at room temperature with high stability, *Sens. Actuators, B*, 403, 135238.

[12] Chen, Q., Zhou, H., Fang, Y., Stieg, A.Z., Song, T.B., Wang, H.H., Xu, X., Liu, Y., Lu, S., You, J., Sun, P., McKay, J., Goorsky, M.S., and Yang, Y., 2015, The optoelectronic role of chlorine in $CH_3NH_3PbI_3(Cl)$-based perovskite solar cells, *Nat. Commun.*, 6 (1), 7269.

[13] Sun, Y., Chen, H., Zhang, T., and Wang, D., 2018, Chemical state of chlorine in perovskite solar cell and its effect on the photovoltaic performance, *J. Mater. Sci.*, 53 (19), 13976–13986.

[14] Al Katrib, M., Planes, E., and Perrin, L., 2022, Effect of chlorine addition on the performance and stability of electrodeposited mixed perovskite solar cells, *Chem. Mater.*, 34 (5), 2218–2230.

[15] Bhattarai, S., Pandey, R., Madan, J., Ansari, M.Z., Hossain, M.K., Amami, M., Ahammad, S.H., and Rashed, A.N.Z., 2024, Chlorine-doped perovskite materials for highly efficient perovskite solar cell design offering an efficiency of nearly 29%, *Prog. Photovoltaics Res. Appl.*, 32 (1), 25–34.

[16] Wang, S., Edwards, P.R., Abdelsamie, M., Brown, P., Webster, D., Ruseckas, A., Rajan, G., Neves, A.I.S., Martin, R.W., Sutter-Fella, C.M., Turnbull, G.A., Samuel, I.D.W., and Jagadamma, L.K., 2023, Chlorine retention enables the indoor light harvesting of triple halide wide bandgap perovskites, *J. Mater. Chem. A*, 11 (23), 12328–12341.

[17] Husain, M., Ullah, A., Algahtani, A., Tirth, V., Al-Mughanam, T., Alghtani, A.H., Sfina, N., Briki, K., Albalawi, H., Amin, M.A., Azzouz-Rached, A., and Rahman, N., 2023, Insight into the structural, mechanical and optoelectronic properties of ternary cubic barium-based $BaMCl_3$ (M = Ag, Cu) chloroperovskites compounds, *Crystals*, 13 (1), 140.

[18] Rahman, N., Husain, M., Tirth, V., Algahtani, A., Alqahtani, H., Al-Mughanam, T., Alghtani, A.H., Khan, R., Sohail, M., Khan, A.A., Azzouz-Rached, A., and Khan, A., 2023, Appealing perspectives of the structural, electronic, elastic and optical properties of $LiRCl_3$ (R = Be and Mg) halide perovskites: A DFT study, *RSC Adv.*, 13 (27), 18934–18945.

[19] Jehan, A., Husain, M., Tirth, V., Algahtani, A., Uzair, M., Rahman, N., Khan, A., and Khan, S.N., 2023, Investigation of the structural, electronic, mechanical, and optical properties of $NaXCl_3$ (X = Be, Mg) using density functional theory, *RSC Adv.*, 13 (41), 28395–28406.

[20] Jehan, A., Husain, M., Sfina, N., Khan, S.N., Rahman, N., Tirth, V., Khan, R., Sohail, M., Rached, A.A., and Khan, A., 2023, First-principles calculations to investigate structural, elastic, electronic, and optical properties of $XSrCl_3$ (X = Li, Na), *Optik*, 287, 171088.

[21] Lakhdar, B., Anissa, B., Radouan, D., Al Bouzieh, N., and Amrane, N., 2023, Structural, electronic, elastic, optical and thermoelectric properties of $ASiCl_3$ (A = Li, Rb and Cs) chloroperovskites: A DFT study, *Opt. Quantum Electron.*, 56 (3), 313.

[22] Khan, N.U., Abdullah, A., Khan, U.A., Tirth, V., Al-Humaidi, J.Y., Refat, M.S., Algahtani, A., and Zaman, A., 2023, Investigation of structural, opto-electronic and thermoelectric properties of titanium based chloro-perovskites $XTiCl_3$ (X = Rb, Cs): A first-principles calculations, *RSC Adv.*, 13 (9), 6199–6209.

[23] Behera, D., Geleta, T.A., Allaoui, I., Khuili, M., Mukherjee, S.K., Akila, B., and Al-Qaisi, S., 2024, First-principle analysis of optical and thermoelectric properties in alkaline-based perovskite compounds $AInCl_3$ (A = K, Rb), *Eur. Phys. J. Plus*, 139 (2), 127.

[24] Ullah, S., Abbas, M., Tariq, S., Batoo, K.M., Rahman, N., Gul, U., Husain, M., Hussain, S., Hasb Elkhalig, M.M.S., and Ghani, M.U., 2024, Density

functional quantum computations to investigate the physical prospects of lead-free chloro-perovskites $QAgCl_3$ (Q = K, Rb) for optoelectronic applications, *Trans. Electr. Electron. Mater.*, 25 (3), 327–339.

[25] Ahmed, M., Bakar, A., Quader, A., Ahmad, R.A., and Ramay, S.M., 2024, First-principles calculations to investigate structural, elastic, mechanical, electronic and optical characteristics of $RbSrX_3$ (X = Cl, Br), *Chem. Phys.*, 581, 112260.

[26] Asif, T.I., Saiduzzaman, M., Hossain, K.M., Shuvo, I.K., Hasan, M.N., Ahmad, S., and Mitro, S.K., 2024, Pressure-driven modification of optoelectronic features of $ACaCl_3$ (A = Cs, Tl) for device applications, *Heliyon*, 10 (5), e26733.

[27] Husain, M., Rahman, N., Albalawi, H., Ezzine, S., Amami, M., Zaman, T., Rehman, A.U., Sohail, M., Khan, R., Khan, A.A., Tahir, T., and Khan, A., 2022, Examining computationally the structural, elastic, optical, and electronic properties of $CaQCl_3$ (Q = Li and K) chloroperovskites using DFT framework, *RSC Adv.*, 12, 32338-32349.

[28] Murshed, M.N., El Sayed, M.E., Naji, S., and Samir, A., 2021, Electronic and optical properties and upper light yield estimation of new scintillating material $TlMgCl_3$: Ab initio study, *Results Phys.*, 29, 104695.

[29] Bouhmaidi, S., Azouaoui, A., Benzakour, N., Hourmatallah, A., and Setti, L., 2022, First-principles calculations on structural, electronic, elastic, optical and thermoelectric properties of thallium based chloroperovskites $TlMCl_3$ (M = Zn and Cd), *Comput. Condens. Matter*., 33, e00756.

[30] Pingak, R.K., Bouhmaidi, S., Harbi, A., Setti, L., Nitti, F., Moutaabbid, M., Johannes, A.Z., Hauwali, N.U.J., and Ndii, M.Z., 2023, A DFT investigation of lead-free $TlSnX_3$ (X = Cl, Br, or I) perovskites for potential applications in solar cells and thermoelectric devices, *RSC Adv.*, 13 (48), 33875–33886.

[31] Pingak, R.K., Johannes, A.Z., Hauwali, N.U.J., and Deta, U.A., 2023, Lead-free perovskites $TlGeCl_xBr_{3-x}$ (x=0,1,2,3) as promising materials for solar cell application: A DFT study, *J. Phys.: Conf. Ser.*, 2623 (1), 012002.

[32] Bouhmaidi, S., Uddin, M.B., Pingak, R.K., Ahmad, S., Rubel, M.H.K., Hakamy, A., and Setti, L., 2023, Investigation of heavy thallium perovskites $TlGeX_3$ (X = Cl, Br and I) for optoelectronic and thermoelectric applications: A DFT study, *Mater. Today Commun.*, 37, 107025.

[33] Rony, J.K., Islam, M., Saiduzzaman, M., Hossain, K.M., Alam, S., Biswas, A., Mia, M.H., Ahmad, S., and Mitro, S.K., 2024, $TlBX_3$ (B = Ge, Sn; X = Cl, Br, I): Promising non-toxic metal halide perovskites for scalable and affordable optoelectronics, *J. Mater. Res. Technol.*, 29, 897–909.

[34] Pingak, R.K., Harbi, A., Moutaabbid, M., Johannes, A.Z., Hauwali, N.U.J., Bukit, M., Nitti, F., and Ndii, M.Z., 2023, Lead-free perovskites $InSnX_3$ (X = Cl, Br, I) for solar cell applications: A DFT study on the mechanical, optoelectronic, and thermoelectric properties, *Mater. Res. Express*, 10 (9), 095507.

[35] Khan, S., Mehmood, N., Ahmad, R., Kalsoom, A., and Hameed, K., 2022, Analysis of structural, elastic and optoelectronic properties of indium-based halide perovskites $InACl_3$ (A = Ge, Sn, Pb) using density functional theory, *Mater. Sci. Semicond. Process.*, 150, 106973.

[36] Han, P., Zhou, W., Zheng, D., Zhang, X., Li, C., Kong, Q., Yang, S., Lu, R., and Han, K., 2022, Lead-free all-inorganic indium chloride perovskite variant nanocrystals for efficient luminescence, *Adv. Opt. Mater.*, 10 (1), 2101344.

[37] Hohenberg, P., and Kohn, W., 1964, Inhomogeneous electron gas, *Phys. Rev.*, 136 (3B), B864–B871.

[38] Hutama, A.S., Hijikata, Y., and Irle, S., 2017, Coupled cluster and density functional studies of atomic fluorine chemisorption on coronene as model systems for graphene fluorination, *J. Phys. Chem. C*, 121 (27), 14888–14898.

[39] Hutama, A.S., Huang, H., and Kurniawan, Y.S., 2019, Investigation of the chemical and optical properties of halogen-substituted *N*-methyl-4-piperidone curcumin analogs by density functional theory calculations, *Spectrochim. Acta, Part A*, 221, 117152.

[40] Pradipta, M.F., Pranowo, H.D., Alfiyah, V., and Hutama, A.S., 2021, Theoretical study of oxygen atom adsorption on a polycyclic aromatic hydrocarbon using density-functional theory, *Indones. J. Chem.*, 21 (5), 1072–1085.

[41] Prasetyo, N., and Pambudi, F.I., 2021, Toward hydrogen storage material in fluorinated zirconium metal-organic framework (MOF-801): A periodic density functional theory (DFT) study of fluorination and adsorption, *Int. J. Hydrogen Energy*, 46 (5), 4222–4228.

[42] Wang, M., Yang, C.X., Leng, X.Y., Chen, Y., Yang, S.B., Li, W., Hong, W., and Xu, Y., 2024, The interface effect on the lithiation of silicon/graphene composites: The first principles study, *Int. J. Quantum Chem.*, 124 (3), e27343.

[43] Hutama, A.S., Marlina, L.A., Chou, C.P., Irle, S., and Hofer, T.S., 2021, Development of density-functional tight-binding parameters for the molecular dynamics simulation of zirconia, yttria, and yttria-stabilized zirconia, *ACS Omega*, 6 (31), 20530–20548.

[44] Das, T., Di Liberto, G., and Pacchioni, G., 2022, Density functional theory estimate of halide perovskite band gap: When spin orbit coupling helps, *J. Phys. Chem. C*, 126 (4), 2184–2198.

[45] Giannozzi, P., Baroni, S., Bonini, N., Calandra, M., Car, R., Cavazzoni, C., Ceresoli, D., Chiarotti, G.L., Cococcioni, M., Dabo, I., Dal Corso, A., de Gironcoli, S., Fabris, S., Fratesi, G., Gebauer, R., Gerstmann, U., Gougoussis, C., Kokalj, A., Lazzeri, M., Martin-Samos, L., Marzari, N., Mauri, F., Mazzarello, R., Paolini, S., Pasquarello, A., Paulatto, L., Sbraccia, C., Scandolo, S., Sclauzero, G., Seitsonen, A.P., Smogunov, A., Umari, P., and Wentzcovitch, R.M., 2009, QUANTUM ESPRESSO: A modular and open-source software project for quantum simulations of materials, *J. Phys.: Condens. Matter*, 21 (39), 395502.

[46] Perdew, J.P., Burke, K., and Ernzerhof, M., 1996, Generalized gradient approximation made simple, *Phys. Rev. Lett.*, 77 (18), 3865–3868.

[47] Birch, F., 1947, Finite elastic strain of cubic crystals, *Phys. Rev.*, 71 (11), 809–824.

[48] Agouri, M., Ouhenou, H., Waqdim, A., Zaghrane, A., Darkaoui, E., Abbassi, A., Manaut, B., Taj, S., and Driouich, M., 2024, Computational study of stability, photovoltaic, and thermoelectric properties of new inorganic lead-free halide perovskites, *Europhys. Lett.*, 146 (1), 16005.

[49] Ati, A.H., Kadhim, A.A., Abdulhussain, A.A., Abed, W.A., Kadhim, K.F., Nattiq, M.A., and Khalaf Al-zyadi, J.M., 2024, Computational study of half-metallic behavior, optoelectronic and thermoelectric properties of new $XAlN_3$ (X = K, Rb, Cs) perovskite materials, *J. Phys. Chem. Solids*, 188, 111899.

[50] Bouhmaidi, S., Pingak, R.K., Azouaoui, A., Harbi, A., Moutaabbid, M., and Setti, L., 2023, *Ab initio* study of structural, elastic, electronic, optical and thermoelectric properties of cubic Ge-based fluoroperovskites $AGeF_3$ (A = K, Rb and Fr), *Solid State Commun.*, 369, 115206.

[51] Jehan, A., Husain, M., Rahman, N., Tirth, V., Sfina, N., Elhadi, M., Shah, S.A., Azzouz-Rached, A., Uzair, M., Khan, A., and Khan, S.N., 2023, Investigating the structural, elastic, and optoelectronic properties of $LiXF_3$ (X = Cd, Hg) using the DFT approach for high-energy applications, *Opt. Quantum Electron.*, 56 (2), 169.

[52] Khan, W., 2024, Computational screening of $BeXH_3$ (X: Al, Ga, and In) for optoelectronics and hydrogen storage applications, *Mater. Sci. Semicond. Process.*, 174, 108221.

[53] Pingak, R.K., 2022., A DFT study of structural and electronic properties of cubic thallium based fluoroperovskites $TlBF_3$ (B = Ge, Sn, Pb, Zn, Cd, Hg, Mg, Ca, Sr, Ba), *Comput. Condens. Matter*, 33, e00747.

[54] Rabbi, S.H., Asif, T.I., Ahmed, M.I., Saiduzzaman, M., and Islam, M., 2024, Unveiling the pressure-driven modulations in $AGeF_3$ (A = Na, Tl) cubic perovskite halides for enhanced optoelectronic performance, *Comput. Condens. Matter*, 38, e00887.

[55] Song, X., Zhao, Y., Wang, X., Ni, J., Meng, S., and Dai, Z., 2023, Strong anharmonicity and high

thermoelectric performance of cubic thallium-based fluoride perovskites $TlXF_3$ (X = Hg, Sn, Pb), *Phys. Chem. Chem. Phys.*, 25 (7), 5776–5784.

[56] Zhang, J., Chen, Y., Chen, S., Hou, J., Song, R., and Shi, Z.F., 2024, First-principles study of mechanical, electronic structure, and optical properties for cubic fluoroperovskite $XMgF_3$ (X=Al, Ga, In, Tl) under high pressure, *Mater. Sci. Semicond. Process.*, 174, 108158.

[57] Bouhmaidi, S., Marjaoui, A., Talbi, A., Zanouni, M., Nouneh, K., and Setti, L., 2022, A DFT study of electronic, optical and thermoelectric properties of Ge-halide perovskites $CsGeX_3$ (X=F, Cl and Br), *Comput. Condens. Matter,* 31, e00663.

[58] Pingak, R.K., Bouhmaidi, S., and Setti, L., 2023, Investigation of structural, electronic, elastic and optical properties of Ge-halide perovskites $NaGeX_3$ (X = Cl, Br and I): A first-principles DFT study, *Physica B*, 663, 415003.

[59] Pingak, R.K., Bouhmaidi, S., Setti, L., Pasangka, B., Bernandus, B., Sutaji, H.I., Nitti, F., and Ndii, M.Z., 2023, Structural, electronic, elastic, and optical properties of cubic $BaLiX_3$ (X = F, Cl, Br, or I) perovskites: An *ab-initio* DFT Study, *Indones. J. Chem.*, 23 (3), 843–862.

[60] Widya, W., Marlina, L.A., Hutama, A.S., and Prasetyo, N., 2023, Role of main group nonmetal dopants on the electronic properties of the TcS_2 monolayer revealed by density functional theory, *J. Electron. Mater.*, 52 (9), 5931–5945.

[61] Zelai, T., Rouf, S.A., Mahmood, Q., Bouzgarrou, S., Amin, M.A., Aljameel, A.I., Ghrib, T., Hegazy, H.H., and Mera, A., 2022, First-principles study of lead-free double perovskites Ga_2PdX_6 (X = Cl, Br, and I) for solar cells and renewable energy, *J. Mater. Res. Technol.*, 16, 631–639.

[62] Born, M., 1940, On the stability of crystal lattices, *I. Math. Proc. Cambridge Philos. Soc.*, 36 (2), 160–172.

[63] Shi, Y.R., Chen, C.H., Lou, Y.H., and Wang, Z.K., 2021, Strategies of perovskite mechanical stability for flexible photovoltaics, *Mater. Chem. Front.*, 5 (20), 7467–7478.

[64] Roknuzzaman, M., Alarco, J.A., Wang, H., Du, A., Tesfamichael, T., and Ostrikov, K., 2019, *Ab initio* atomistic insights into lead-free formamidinium based hybrid perovskites for photovoltaics and optoelectronics, *Comput. Mater. Sci.,* 169, 109118.

[65] Ghaithan, H.M., Alahmed, Z.A., Qaid, S.M.H., and Aldwayyan, A.S., 2021, Density functional theory analysis of structural, electronic, and optical properties of mixed-halide orthorhombic inorganic perovskites, *ACS Omega*, 6 (45), 30752–30761.

[66] Pugh, S.F., 1954, XCII. Relations between the elastic moduli and the plastic properties of polycrystalline pure metals, *London, Edinburgh, Dublin Philos. Mag. J. Sci.*, 45 (367), 823–843.

[67] Ahmad, S., Ur Rehman, J., Tahir, M.B., Alzaid, M., and Shahzad, K., 2023, Investigation of external isotropic pressure effect on widening of bandgap, mechanical, thermodynamic, and optical properties of rubidium niobate using first-principles calculations for photocatalytic application, *Opt. Quantum Electron.*, 55 (4), 346.

[68] Tripkovic, V., Hansen, H.A., Garcia-Lastra, J.M., and Vegge, T., 2018, Comparative DFT+U and HSE study of the oxygen evolution electrocatalysis on perovskite oxides, *J. Phys. Chem. C*, 122 (2), 1135–1147.

[69] Råsander, M., and Moram, M.A., 2015, On the accuracy of commonly used density functional approximations in determining the elastic constants of insulators and semiconductors, *J. Chem. Phys.*, 143 (14), 144104.

[70] Ali, M.A., Alothman, A.A., Mushab, M., and Faizan, M., 2024, Optoelectronic and thermoelectric properties of novel stable lead-free cubic double perovskites A_2NaIO_6 (A = Ca, Sr) for renewable energy applications, *Phys. Chem. Chem. Phys.*, 26 (4), 3614–3622.

[71] Ayyaz, A., Murtaza, G., Usman, A., Sfina, N., Alshomrany, A.S., Younus, S., Saleem, S., and Urwa-tul-Aysha, 2024, Evaluation of physical properties of $A_2ScCuCl_6$ (A = K, Rb, and Cs) double perovskites *via* DFT framework, *J. Inorg. Organomet. Polym. Mater.*, Article in press.

[72] Bouhmaidi, S., Pingak, R.K., and Setti, L., 2023, First-principles investigation of electronic, elastic,

optical and thermoelectric properties of strontium-based anti-perovskite Sr_3MN (M= P and As) for potential applications in optoelectronic and thermoelectric devices, *Moroccan J. Chem.*, 11 (4), 1254–1265.

[73] Harbi, A., and Moutaabbid, M., 2022, First-principles investigation of structural, elastic, thermoelectric, electronic, and optical properties of ordered double perovskite Ba_2MWO_6 (M = Mg, Zn, and Cd), *J. Supercond. Novel Magn.*, 35 (11), 3447–3456.

[74] Hayat, M.S., and Khalil, R.M.A., 2024, Computational predictions of optoelectronic energy materials Cs_2SiBr_6 Cs_2GeBr_6 & Cs_2SnBr_6 for phenomenal photovoltaic applications; A first principles study, *Comput. Theor. Chem.*, 1235, 114532.

[75] Assiouan, K., Marjaoui, A., EL Khamkhami, J., Zanouni, M., Ziani, H., Bouchrit, A., and Achahbar, A., 2024, Theoretical investigation of Rb_2AuBiX_6 (X=Br, cl, F) double perovskite for thermoelectric and optoelectronic applications, *J. Phys. Chem. Solids*, 188, 111890.

[76] Bouhmaidi, S., Harbi, A., Pingak, R.K., Azouaoui, A., Moutaabbid, M., and Setti, L., 2023, First-principles calculations to investigate lead-free double perovskites $CsInSbAgX_6$ (X = Cl, Br and I) for optoelectronic and thermoelectric applications, *Comput. Theor. Chem.* 1227, 114251.

[77] Harbi, A., Bouhmaidi, S., Pingak, R.K., Setti, L., and Moutaabbid, M., 2023, First-principles calculations to investigate optoelectronic, thermoelectric and elastic properties of novel lead-free halide perovskites $CsRbPtX_6$ (X = Cl, Br and I) compounds for solar cells applications, *Physica B*, 668, 415242.

[78] Hemidi, D., Seddik, T., Benmessabih, T., Batouche, M., Ouerghui, W., Abdallah, H.B., Surucu, G., and Ahmad, S., 2023, Is Rb_2PtX_6 (X = Cl, Br, and I) a promising Pb-free vacancy-ordered double perovskites for photoelectrochemical water splitting applications?, *Appl. Phys. A*, 129 (11), 762.

[79] Murtaza, H., Ain, Q., Munir, J., Ghaithan, H.M., Ahmed Ali Ahmed, A., Aldwayyan, A.S., and Qaid, S.M.H., 2024, Effect of bandgap tunability on the physical attributes of potassium-based K_2CuBiX_6 (X = I, Br, Cl) double perovskites for green technologies, *Inorg. Chem. Commun.*, 162, 112206.

[80] Ou, T., Jiang, W., Zhuang, Q., Yan, H., Feng, S., Sun, Y., Li, P., and Ma, X., 2023, First-principles study of electronic and optical properties of lead-free halide double perovskite Cs_2RbSbX_6 (X=Cl, Br, I), *Physica B*, 665, 415050.

[81] Peng, C., Wei, J., Wu, J., Ma, Z., Qiao, C., and Zeng, H., 2024, Modulation mechanism of electronic and optical properties of Cs_2SnX_6 (X = Cl, Br and I) under hydrostatic or uniaxial pressure, *Funct. Mater. Lett.*, 17 (3), 2451012.

[82] Johannes, A.Z., Pingak, R.K., and Bukit, M., 2020, Tauc plot software: Calculating energy gap values of organic materials based on Ultraviolet-Visible absorbance spectrum, *IOP Conf. Ser.: Mater. Sci. Eng.*, 823 (1), 012030.

[83] Reddy, R.R., Gopal, K.R., Narasimhulu, K., Reddy, L.S.S., Kumar, K.R., Balakrishnaiah, G., and Kumar, M.R., 2009, Interrelationship between structural, optical, electronic and elastic properties of materials, *J. Alloys Compd.*, 473 (1), 28–35.

[84] Li, K., Kang, C., and Xue, D., 2012, Electronegativity calculation of bulk modulus and band gap of ternary ZnO-based alloys, *Mater. Res. Bull.*, 47 (10), 2902–2905.

[85] Biswas, A., Alam, M.S., Sultana, A., Ahmed, T., Saiduzzaman, M., and Hossain, K.M., 2021, Effects of Bi and Mn codoping on the physical properties of barium titanate: Investigation via DFT method, *Appl. Phys. A,* 127 (12), 939.

[86] Penn, D.R., 1962, Wave-number-dependent dielectric function of semiconductors, *Phys. Rev.*, 128 (5), 2093–2097.

[87] Lamichhane, A., and Ravindra, N.M., 2020, Energy gap-refractive index relations in perovskites, *Materials*, 13 (8), 1917.

[88] Hassan, B., Irfan, M., Aslam, M., and Buntov, E., 2024, The electronic structure, electronic charge density, optical and thermoelectric properties of Mo and Rh based triple perovskite semiconductors $Ba_3CaNb_2O_9$ for low-cost energy technologies, *Opt. Quantum Electron.*, 56 (3), 398.

[89] Rehman, M.A., ur Rehman, Z., Usman, M., Farrukh, U., Alomar, S.Y., Ahmad, N., Ahmad, T., Farid, A., and Hamad, A., 2024, Pressure-induced modulation of structural, electronic, and optical properties of $LiCaF_3$ fluoro perovskite for optoelectronic applications, *Solid State Commun.*, 380, 115447.

[90] Valizadeh, S., Shokri, A., Sabouri-Dodaran, A., Fough, N., and Muhammad-Sukki, F., 2024, Investigation of efficiency and temperature dependence in $RbGeBr_3$-based perovskite solar cell structures, *Results Phys.*, 57, 107351.

[91] Ajay, G., Ashwin, V., Sirajuddeen, M.M.S., and Alam, A., 2024, Theoretical investigation of structural, electronic, elastic, and optical properties of rubidium-based perovskites RbSrX3 (X = Cl, Br) for optoelectronic device applications – A DFT study, *Physica B*, 682, 415858.

[92] Liang, Y., Cui, X., Li, F., Stampfl, C., Ringer, S.P., and Zheng, R., 2021, First-principles investigation of intrinsic point defects in perovskite $CsSnBr_3$, *Phys. Rev. Mater.*, 5 (3), 035405.

[93] Liang, Y., Cui, X., Li, F., Stampfl, C., Huang, J., Ringer, S.P., and Zheng, R., 2021, Hydrogen-anion-induced carrier recombination in $MAPbI_3$ perovskite solar cells, *J. Phys. Chem. Lett.*, 12 (43), 10677–10683.

[94] Liang, Y., Cui, X., Li, F., Stampfl, C., Ringer, S.P., Yang, X., Huang, J., and Zheng, R., 2023, Origin of enhanced nonradiative carrier recombination induced by oxygen in hybrid Sn perovskite, *J. Phys. Chem. Lett.*, 14 (12), 2950–2957.

[95] Liang, Y., Cui, X., Li, F., Stampfl, C., Ringer, S.P., and Zheng, R., 2022, Atomic and molecular hydrogen impurities in hybrid perovskite solar cells, *J. Phys. Chem. C*, 126 (4), 1721–1728.